LOW-FIELD NMR METHODS APPLIED TO THE CHARACTERIZATION OF COCONUT CREAM

Jürgen H. Antony [1], Edme H. Hardy [2,], Nikolaus Nestle [3]*

[1] Escuela de Química, Universidad de Costa Rica (UCR), 11501-2060 San José, Costa Rica.
[2] Karlsruhe Institute of Technology (KIT), CS, IMVM, 76131 Karlsruhe, Germany.
[3] BASF SE, GKC/R-G201, 67056 Ludwigshafen, Germany.

Abstract

Several low-field NMR methods in combination were applied to investigate the flow properties, stability and drying behavior of coconut cream. From measurements of NMR relaxation in confined samples, insight into the creaming stability of the emulsions was obtained in a non-invasive manner; the multiphase structure of a creamed emulsion was visualized with 1D-NMR imaging; the flow behavior of the (homogenized) emulsion was measured by means of rheo-NMR, leading to a power law index 0.61 in an Ostwald-de-Waele model. The drying and the role of creaming in this process were followed with depth resolution through profiling NMR.

Resumen

Las propiedades de flujo, la estabilidad y el comportamiento de secado de leche de coco se investigó por varios métodos de RMN a campo bajo. Mediante estas técnicas se obtuvo información sobre la estabilidad de las emulsiones de manera no invasiva. Múltiples fases por imagen se midieron mediante resonancia magnética de una dimensión y propiedades reométricas de muestras homogenizadas por rheo-RMN. Por otro lato, un índice de potencia de 0.61 se encontró con la aplicación del modelo de Ostwald-de-Waele.

I. INTRODUCTION

Coconut cream that forms on aqueous extraction of solid coconut endosperm is an important ingredient in Asian cuisine [1,2]. The major components are water and fat; the minor components are carbohydrates and proteins. The fat content typically ranges from 15 to 35 %, the water content from 55 to 75 %, the protein content from 2 to 4 %, and the carbohydrate content

---

* Corresponding author: Edme.Hardy@kit.edu

from 2.5 to 5 % [3]. It is basically an emulsion of oil in water that is stabilized by proteins, which tends to separate into two phases on creaming.

Low-field nuclear-magnetic-resonance (NMR) bench-top instruments are established in food science and technology, e.g. for the determination of the content of solid fat, the distribution of droplet size, or the content of oil and moisture [4,5]. High-field magnetic-resonance-imaging (MRI) scanners equipped with three-axis magnetic-field gradient systems allow more sophisticated investigations [6,7], but their application is limited by the large investment and operating costs as well as by the demanding site requirements. The present work summarizes the application of innovative low-field NMR methods to the characterization of coconut cream as an example of a complicated food sample. These NMR methods are sensitive not only to the content of hydrogen nuclei in fat and water but also, through analysis of the signal relaxation, to the microstructure of the emulsion phases. With the addition of one to three magnetic-field gradient axes, spatially resolved NMR methods can provide information on the macroscopic heterogeneity inside an emulsion sample [8]. Gradient methods enable also a study of flow and self-diffusion, allowing inferring a distribution of the droplet size or the rheological properties. We applied both measurements in a homogeneous field formed in a permanent-magnet system with optional pulsed magnetic-field gradients and unilateral profiling NMR with a static magnetic-field gradient. The latter method offers effective possibilities for the study of the drying of thin emulsion samples under atmospheric storage in which the stability of the emulsion is affected additionally by the variation of water content.

II.   MATERIALS AND METHODS

Test fluids

The coconut creams tested in this work were commercially available products of brands 'Alnatura' (ecological product, fat content 22 %, origin in Sri Lanka), 'Chaokoh' (fat content 17 %, origin in Thailand) and 'Aroy-D' (fat content 17 %, origin in Thailand). They became homogenized on shaking and used without further treatment.

NMR instruments

NMR relaxation, 1D- imaging, and rheo-TD-NMR spectra were recorded (Bruker Minispec mq10rheo benchtop NMR Analyzer; Bruker Optics, Rheinstetten, Germany) at resonance frequency 9.96 MHz for hydrogen nuclei. A static magnetic field 0.235 T was generated with a permanent magnet (pole gap 50 mm). Experiments with pulsed magnetic-field gradients were performed with a gradient amplifier (Bruker Great 60) delivering a current up to 60 A to the gradient coils, which yields a magnetic-field gradient up to 3 T/m; the gradient was oriented vertically so that both 1D-projection imaging along the direction of gravity and flow encoding in this direction were practicable. NMR pulse sequences were used as provided (Bruker) or written in ExpSpel (part of the minispec software).

NMR spectra of the depth profile were recorded (ACT Profile NMR Mouse PM 5; ACT, Aachen, Germany, equipped with a HP lift setup and operating at proton NMR frequency 19.8 MHz). The static linear-background gradient was 22 T/m. A console (Bruker minispec mq20, Bruker Optics, Rheinstetten, Germany) was used with this NMR setup. To minimize problems with the thermal drift of the magnet system, we housed the magnet and the lift setup in an

insulating box made of extruded polystyrene foam (Styrodur ®, 5 cm), that was heated to 30 °C with warm water circulating through a heating loop (copper tube) inside the foam box.

Experiment

NMR relaxation and 1D imaging experiments were conducted with samples contained in test tubes (outer diameter 10 mm); the tube axis was oriented vertically. Relaxation in flowing samples and the velocity probability-density function were measured for samples pumped through a glass tube (diameters inner 4 mm, outer 7 mm); the NMR measuring volume was accessible from the top and bottom of the analyzer. A syringe pump (KDS 210 CE, KD Scientific, Holliston, MA USA) provided a constant rate of flow. Drying was performed in a Petri dish filled with a layer of coconut cream (thickness about 1.1 mm). To avoid perturbations from ambient air currents, we placed an open plastic tube (diameter 10 cm, length 1 m) around the Petri dish.

NMR Methods

The transverse relaxation was measured on acquisition of an echo train with Carr–Purcell–Meiboom–Gill (CPMG) pulse sequences. As is customary in low-field NMR, only the maximum of each echo was evaluated; several thousand echoes were typically generated. Several scans were accumulated to improve the ratio of signal to noise and to diminish experimental artifacts. To adjust the repetition interval between individual scans, we analyzed the longitudinal relaxation on measuring the inversion recovery. For 1D-imaging, we used a spin-echo experiment with pulsed-gradient frequency encoding. Relaxation contrast was introduced on varying either the echo period during which transverse relaxation occurred or the repetition delay, with increasing magnetization saturation to increase the ratio of the longitudinal relaxation time and repetition time. The velocity probability-distribution function (VPDF) was measured with a pulsed-gradient spin-echo sequence (PGSE). Both the relaxation of flowing samples and the pulse sequence for NMR depth profiling were measured with the CPMG sequence.

Evaluation of data

In a CPMG echo train acquired to investigate the transverse NMR relaxation, the rate of signal decrease shortly after the signal excitation is larger than at later times. The ratio of signal to noise in the echo train correspondingly decreases with increasing time. A moving average with increasing window width of some sort is accordingly indicated. For our measurements on the samples in test tubes and on flowing samples, the following simple averaging scheme proved to be suitable. The first echo-data point is used without modification. The average of the following pair of echo intensities is used next. The average for the following triple is then calculated, and so on; i. e. the number of points per averaged intensity is incremented by one for each new averaged data point. The times of the original data set are averaged according to the same procedure. The increase of interval length is recognizable in Figure 2 (sample in test tube) or Figure 5 (flowing sample); these semi-logarithmic plots also make evident that the data sets reduced in this manner exhibit a satisfactory ratio of signal to noise for all times, although the signal range varies over more than three orders of magnitude. As preliminary averaging in a data reduction step, odd and even echoes can be averaged. Depending on the complexity of the decay curve, a single exponential or a sum of two or three exponentials is fitted (MATLAB, The MathWorks, Inc., Natick, MA USA) to the data. The initial amplitude of each exponential is directly related to the contributing number of nuclear spins. The time constant, i. e. transverse relaxation time T_2, is related to the molecular dynamics involved.

One-dimensional parameter-weighted projection images along the symmetry axis of samples in test tubes were obtained as the magnitude of the Fourier transform of the frequency-encoded spin-echo signal.

The velocity probability-density function $f(v)$ was obtained on Fourier transformation of the PGSE data, and was integrated to the cumulative velocity distribution $F(v)$ using the trapezoidal rule. For fully developed isothermal laminar capillary flow of a macroscopically homogeneous fluid, the cumulative distribution up to velocity $v(r)$ is related to the corresponding coordinate r and the tube radius R by

$$F(v) = \int_0^v f(v')\mathrm{d}v' = \frac{\pi R^2 - \pi r^2}{\pi R^2} \tag{1}$$

This equation was solved for the inverse velocity profile:

$$r(v) = R\sqrt{1 - F(v)} \tag{2}$$

The flow profile resulting from a given rheological model is eventually fitted to the profile measured in the NMR spectra to obtain the parameters of the model [9-11].

In a depth-profile NMR setup, the signal decay measured with a CPMG sequence is determined not only by relaxation but also by diffusion, because of the strong background magnetic-field gradient G. The resulting rate $1/T_{2\,app}$ of relaxation is the sum of the relaxation rate $1/T_{2o}$ in a homogeneous magnetic field and a diffusive contribution:

$$\frac{1}{T_{2app}} = \frac{1}{T_{2o}} + \frac{1}{12}\gamma^2 G^2 \mathrm{D}t_e^2 \tag{3}$$

The gyromagnetic ratio g is a property of the nuclear spin. For the shortest technically feasible echo time t_e on the NMR profiling system (which is 56.1 µs for a slice of thickness 100 µm), which yields an apparent relaxation time for water (D=2.3 10^{-9} m^2/s, 25°C [12]) about 50 ms (instead of 3 s). In contrast, the impact of eqn (1) on the oil phase (diffusion coefficients about 8.6 10^{-11} m^2/s [13]) is still negligible. Working with longer echo times, we can further shorten the effective relaxation time of the water phase. In this work, an echo time 156.1 µs was used, corresponding to an apparent relaxation time of free water of order 6.5 ms. The time for recording each profile was about 6 min.

Because of the measurement conditions in unilateral NMR, the ratio of signal to noise in depth-profiling NMR experiments tends to be small (see figure 1 for example). To facilitate an evaluation of the relaxation curves, we subjected the data to a sequential binning procedure as a first step of the evaluation. The binned data points are plotted in figure 1 with the measured curve. The first four bins were averaged over 8 measured points, the next two bins over 16 points and the last six bins over 32 points. Furthermore, we computed profiles of the average of all measured points at each depth (with an increased ratio of signal to noise) to identify possible heterogeneities of the profiles.
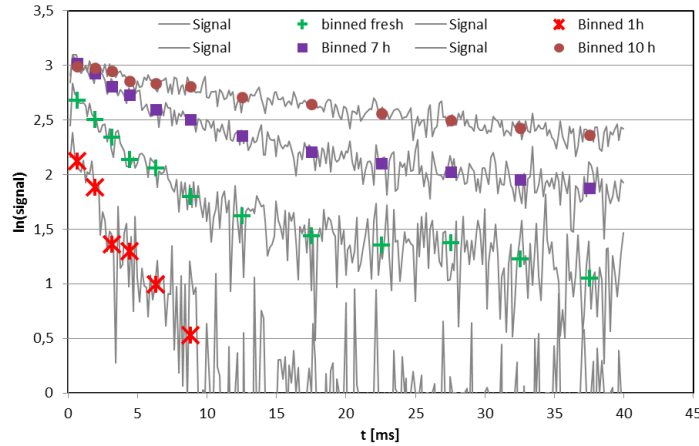
FIGURE 1. Exemplary raw CPMG-signal decay curves and binned data from depth profiling NMR experiments on a drying coconut cream sample at fixed height over the sensor; for details see section 3.6.

III.   RESULTS AND DISCUSSION

Measurements of relaxation in homogeneous emulsion and separated phases

We studied, as reference, the transverse relaxation of a fresh and homogenized coconut-cream sample and, as test cases, samples of the upper and the lower phases after creaming. Figure 2 shows that the relaxation of the fresh sample and of the creamed upper phase are multiply exponential whereas the relaxation decay of the lower phase is almost singly exponential.

The singly exponential fit

$$I(t) = a \exp(- t / T_2)$$

of the data of the lower phase yields

$a = 77.7(1)$ and $T_2 = 534(1)$ ms.

The triexponential fit

$$I(t) = a \exp(- t / T_{2a}) + b \exp(- t / T_{2b}) + c \exp(- t / T_{2c})$$

of the data of the upper phase yields

$a = 14(4)$, $T_{2a} = 74(8)$ ms, $b = 31(2)$, $T_{2b} = 169(24)$ ms, $c = 21(5)$, and $T_{2c} = 348(21)$ ms,

and for the mixture,

$a = 12(3)$, $T_{2a} = 81(7)$ ms, $b = 23(1)$, $T_{2b} = 195(23)$ ms, $c = 27(3)$, and $T_{2c} = 440(13)$ ms,

in which numbers in parentheses are uncertainties referred to the corresponding last digits of the quoted results. Weights a, b and c have arbitrary units, with 100 indicating a linear range of the measuring system.

The lower phase consists of mainly water with a corresponding singly exponential signal decay. Compared to pure water with a relaxation period a few seconds, the time constant becomes half a second due to salt and other dissolved substances. The creamed upper phase consists of various components with varied relaxation times. A biexponential fit deviates systematically from the experimental data, but a triexponential fit is sufficiently flexible to describe adequately the data; further exponentials result in ample uncertainties. The weights have the same order of magnitude. Adjacent time constants differ approximately by a factor two and are invariably smaller than the time constant of the lower phase. The results of the fit for the mixture reflect the results obtained on the separate phases. Compared with the creamed phase, the weight of the longest relaxation time is enhanced and all time constants are increased.
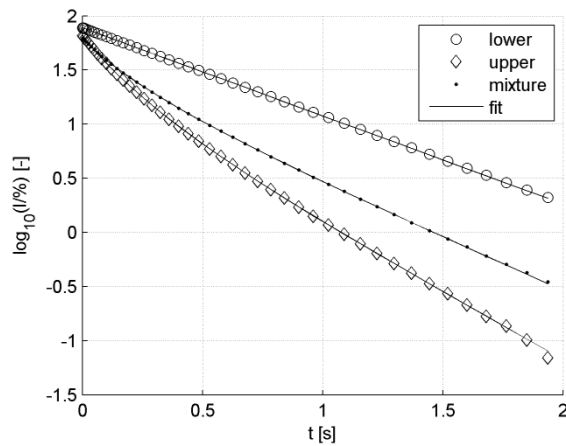
FIGURE 2. Transverse relaxation of isolated phases of creamed coconut cream and the homogeneous emulsion

Relaxation-weighted measurements on creamed samples with one-dimensional spatial resolution

One-dimensional projection images with varied echo times and relaxation delays were applied to the creamed sample; figure 3 shows the results. For both transverse and longitudinal relaxation weighting, the separation in two phases is clearly visible. Transverse-relaxation-weighted images were acquired with a relaxation delay 3000 ms to ensure full relaxation of the sample; see figure 3 left. The echo time (TE) was varied from 6 ms to 192 ms. For echo times from 6 ms to 96 ms, the signal amplitude for the lower part of the sample is larger; the reason is that the water-rich lower part of the sample has a longer transverse relaxation time than the fat-rich upper part, so that in the detected echo the remaining magnetization for the water- rich part is larger than that for the fat-rich part. At an echo time 192 ms, the contrasting situation has an inverted signal amplitude with the lower part of the sample being smaller than for the upper part of the sample. At this long echo time, the more rapid self-diffusion of water in the presence of magnetic-field background gradients enhanced the apparent transverse relaxation.
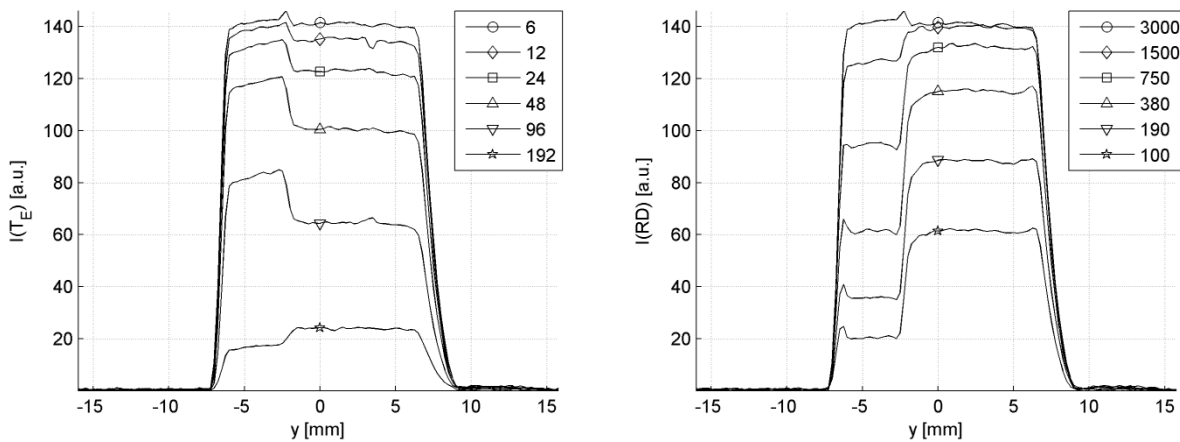

FIGURE 3. One-dimensional parameter-weighted projection images of a creamed sample. The vertical axis is denoted as the y axis. Left: Variation of T₂ weighting; curves are numbered according to the echo times used

in the various experiments. Right: Variation of T_1 weighting. Curves are numbered according to the various relaxation delays used.

Longitudinal-relaxation-weighted images were made with echo time 6 ms; the relaxation delay (RD) was varied from 100 ms to 3000 ms, see figure 3 right. When the relaxation delay is small, as there is insufficient duration for the magnetization to come to equilibrium the intensity of the detected echo is decreased. For the lower part of the sample this effect is more significant than for the upper part because of the longer relaxation time of the water-rich lower part. No contrast inversion is observed during this period as the longitudinal relaxation is insensitive to diffusion.

Especially at the smallest relaxation delays, in the right side of figure 3 an additional feature is observed at the bottom of the tube, located at approximately -7 mm. The intensity is enhanced with respect to the remaining lower phase because of the more rapid longitudinal relaxation. Inspection of the left side of figure 3 at larger echo times reveals a smaller intensity in this region, because of more rapid transverse relaxation. These observations are explicable with a sediment at the bottom of the tube. The signal at the free surface about 9 mm is blurred by the meniscus, but a relaxation behavior is discernible at the surface slightly different from the rest of the upper phase. Likewise the projection with least relaxation weighting (either side of figure 3) reveals a slightly enhanced signal at the interface between lower and upper phases.

Monitoring of creaming with measurements of NMR relaxation

The creaming of one sample was also monitored with measurements of the non-imaging transverse relaxation (Figure 4). This relaxation was found to be more nearly triexponential than biexponential. The triexponential fit results are consistent with an interpretation including hydrogen nuclei in environments of three kinds. Hydrogen nuclei in fat molecules have the largest rate of relaxation, essentially independent of the microstructure within the sample. For the hydrogen of free water formed after phase separation has begun, the relaxation rate is least. The rates of relaxation for water in the diminishing emulsion phase have intermediate values, being sensitive to the emulsion microstructure. As figure 4 shows, the amount of free water was still increasing and the amount of water in the remaining emulsion phase still decreasing after 900 min. The contribution obtained from the hydrogen in fat molecules was nearly constant, as expected. The slight increase towards longer times might be due to fitting artifacts arising from the decreasing difference in the relaxation times for emulsion water and fat.
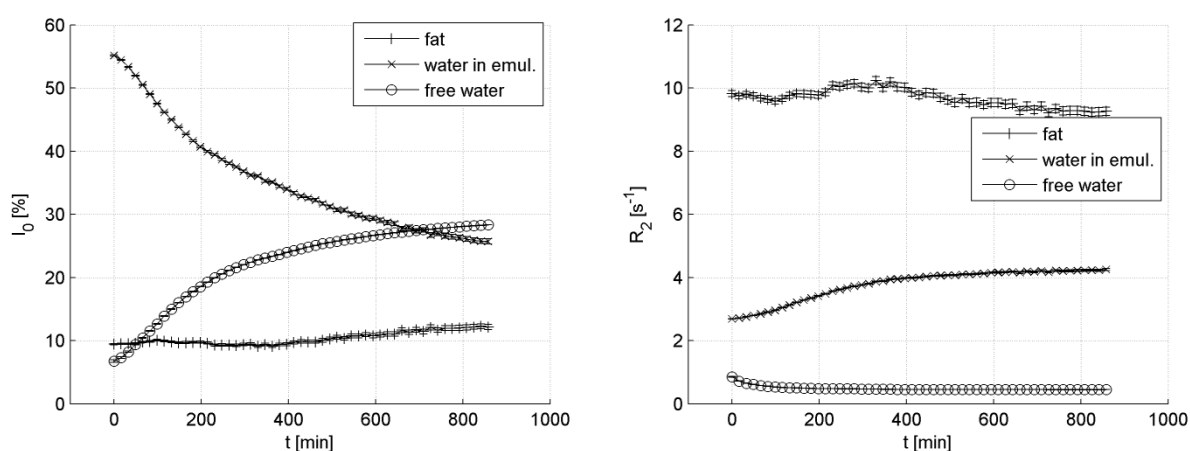
FIGURE 4. Weights and relaxation rates from triexponential fits to CPMG relaxation data as a function of creaming duration for an initially homogeneous sample of coconut cream (Chaokoh). Weights

and relaxation rates are consistently attributed to fat, free water forming as phase separation progresses and water remaining in a diminishing emulsion phase.

In-line rheo-TD-NMR measurements on pipe flow

Figure 5 shows the CPMG signal decay under flow for varied flow rates. Figure 6 shows the intensity relative to that without flow; time is normalized by the respective mean residence duration in the detection area. In [10] a master curve for this data representation is calculated from the velocity-dependent cross-correlation of excitation-efficiency and detection-sensitivity profiles weighted by the velocity probability-density function. If these functions are known and if the model is applicable, relaxation-decay functions measured online under flow can be corrected to the decay function without flow for standard analysis. In figure 6, small differences between the curves are still visible. Further investigation is in progress to determine the origin of the remaining differences in such experiments.
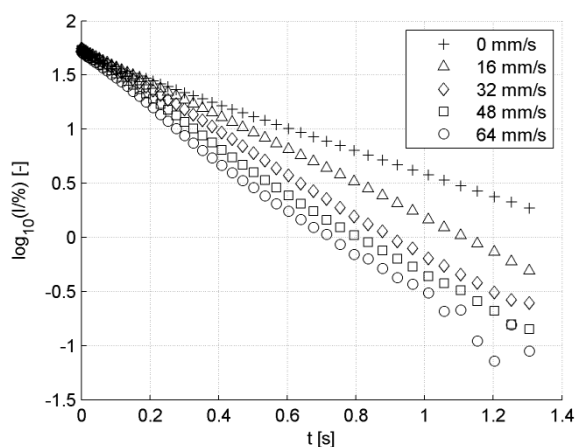

FIGURE 5. CPMG signal decay at varied flow rates (Aroy-D). The respective mean velocity is indicated in the legend.
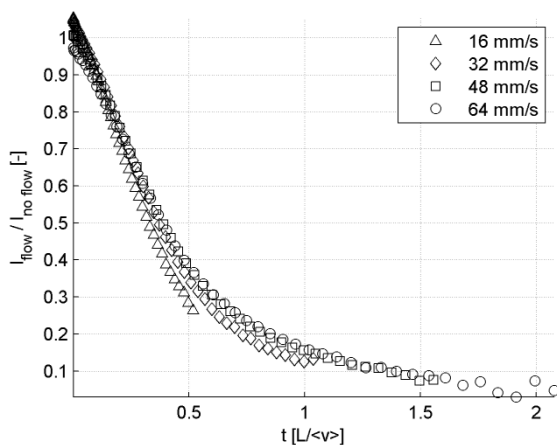

FIGURE 6. Intensities of CPMG echoes of varied flow rates relative to intensities without flow and time normalized to the mean residence duration in the sensitive region of the NMR system.

PGSE measurement of velocity probability density

We analyzed the flow profile of a coconut cream (Aroy-D) measured with PSGE NMR shown in figure 7 on fitting the profile of an Ostwald-de Waele fluid, resulting in a power law index 0.61; that this value is less than unity corresponds to a shear-thinning behavior. To verify the method, this experiment was repeated with olive oil, which resulting in a fitted power law index 0.96, i.e. nearly unity, corresponding to a Newtonian fluid.
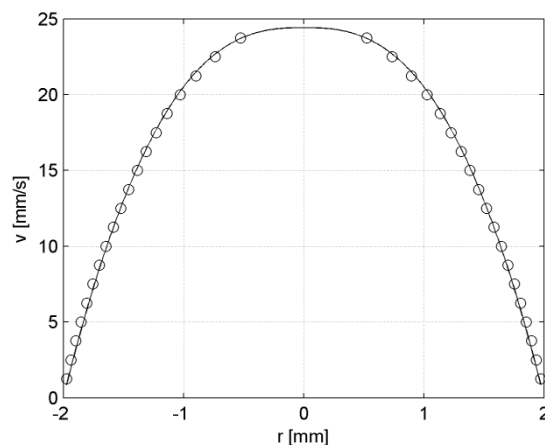
FIGURE 7. Velocity profile of coconut cream (Aroy-D) at flow rate 12 mL/min measured with PGSE-NMR (circles) and fit of an Ostwald de Waele velocity profile with power law index n = 0.61.

In other measurements of coconut cream the VPDF exhibited several maxima; this behavior was likely caused by phase separation that led to inhomogeneous flow. To verify the power-law index, we measured the viscosity (of Aroy-D) dependent on shear rate with a rotational viscometer (Haake RS 150, Z20-DIN). At 313 K a power law index 0.67 was found, in reasonable agreement with the NMR result.

Among reports of the viscosity of coconut cream with rotational viscometers in the literature, Simuang et al [14] studied the viscosity of various coconut creams with fat contents 15-30 % in a temperature range 70-90 ⁰C and found significant effects on the rheological properties of the coconut cream; these authors reported a shear thinning behavior with a power law index between 0.756 and 0.923. Peamprasart and Chiewchan also found this behavior in investigations including a preheating treatment [15]; they obtained a power-law index between 0.713 and 0.930. Jirapeangtong et al. [16] studied the effect of coconut sugar and stabilizing agents on the apparent viscosity of a high-fat coconut cream and found a power law index between 0.63 and 0.84. As the latter work was conducted near 23 ºC, the rheology is expected to be similar to our findings, as is the case.

Profile NMR measurements on drying samples

Figure 8 shows the depth profiles of an average CPMG-signal obtained at an interval about 30 min on a drying sample of coconut cream (Aroy D) in an open Petri dish. Even these crude data allow discerning several phases of drying. Almost immediately after pouring the coconut cream into the Petri dish, creaming begins, leading to two phases well separated after about 1 h. Over the next few hours, the properties of the creamed layer seem to alter little while the thickness of the lower phase decreases. After about 6 h, the signal intensity of the remaining material increases again and after about 10 h a final stage seems to arise. To simplify the figures, we present a

detailed evaluation with sequential binning on the example of the four representative profile data sets marked in figure 8.

In figure 1, the signal-decay curves measured in the slice at height 2300 μm over the sensor are given for these four drying times. As is visible from the structure of the signal decay curves, the signal decay in a fresh sample is clearly non-exponential. Based on the rationale given in section 2.5, the rapidly decaying component is attributed to water; the slow-relaxing component is due to the fat. The separation between water inside the emulsion and bulk water as described in section 3.3 is inapplicable here as the diffusion effect is much stronger than the effect of varying rates of relaxation, but the decreased sensitivity of confined water to diffusion effects might result in the emulsion water contributing to the fat signal at later drying stages. Figure 9 shows the binned data with a biexponential fit. After 1 h, the slice contains a water-rich phase, explaining the small amplitude and rapid relaxation. At 7 and 10 h, the slice is filled with a fat-rich creamed phase.
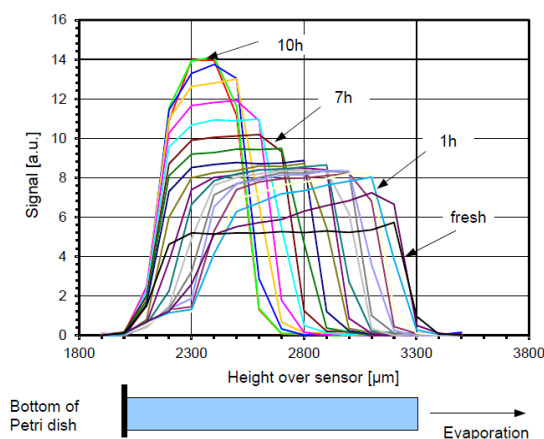

FIGURE 8. Average CPMG-signal depth profiles from a coconut cream sample drying in a Petri dish. In the lower part of the figure, the drying geometry is sketched.
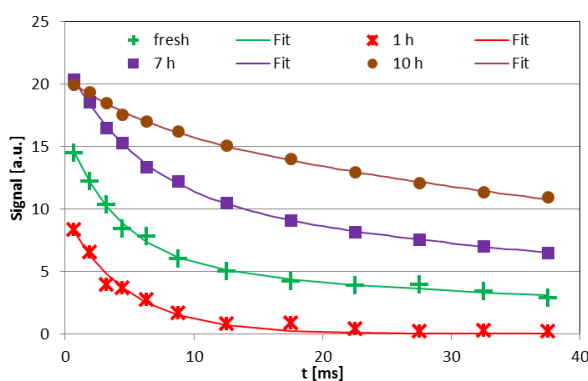

FIGURE 9. Binned signal decay curves at a given depth (2300 μm) computed from the signals in figure 1 with biexponential fits.

As most data sets did not relax to zero (to keep the duty cycle of the profiling NMR setup sufficiently small, only 256 echoes were acquired during the given repetition period), biexponential fitting of the data is not an ideal approach to quantify the amount of slowly relaxing

components that are attributed to the fat phase. Instead, a singly exponential evaluation of the long time 'tail' of the binned data sets was performed, leading to the profiles shown in figure 10. Figure 11 gives the spatially averaged long-time amplitude and relaxation time obtained from the creamed layer. As this graph shows, the separate phases of the creaming and drying of the coconut cream are readily discernible. After rapid initial creaming (about 1 h), the NMR properties remained almost constant with a slightly increased amplitude and a slightly decreased relaxation time. After about 7 h, the amplitude began to increase again, much more strongly. This increase was then followed by an increased relaxation time that arose after about 8 h. The findings in the NMR behavior are attributed to the following effects:

- enrichment of the fat phase due to creaming in the first hour;
- altered microstructure of the cream layer leading to water molecules confined into structures smaller than 1 μm (which are less sensitive to diffusion effects in the background gradient and thus contribute to the long-time signal) along with evaporation of the bottom water phase through the creaming layer;
- evaporation of water from the creamed layer leading to an increasing coalescence of the fat droplets;
- maturing of the fat layer with a local separation between components of distinct mobility (leading to further increased T2 time of the 'mobile' signal and a decreased amplitude through formation of more rapidly relaxing and more 'solid' fat domains).
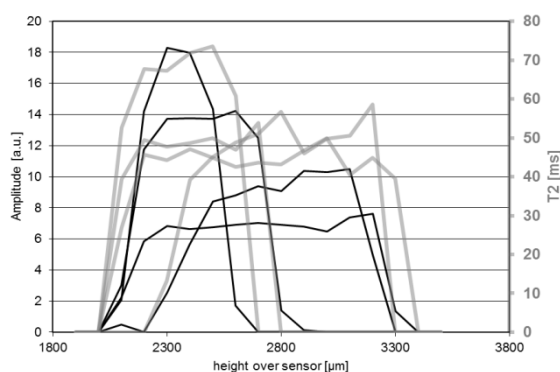
FIGURE 10. Amplitude profiles (black) and relaxation times (gray) for the slowly relaxing signal window determined from regression over the 'tail' data.
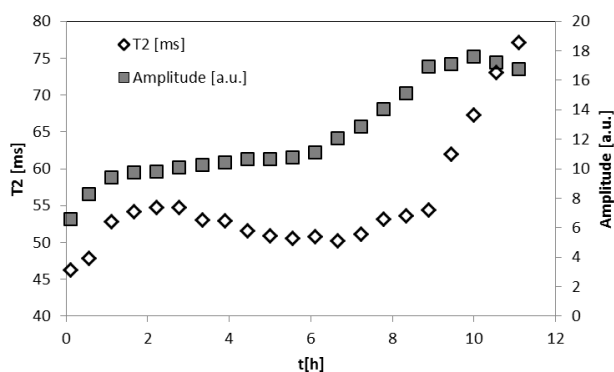
FIGURE 11. Spatially averaged long-time signal amplitude and T2-value for the creamed layer as a function of drying duration

In summary, our results show that various low-field NMR methods in combination provide insight into the flow properties and creaming behavior of food emulsions such as coconut cream. A particular advantage of the NMR methods is their non-invasive nature: the flow-through setup is applicable even as an online tool. Profiling NMR, in contrast, provides an excellent tool to study creaming and the coalescence of fatty emulsions because of its open geometry and the potential to control the environment of the drying emulsion almost independently of the NMR experiment.

IV.   REFERENCES

[1]   Seow, C. C., & Gwee, C. N. Coconut milk: chemistry and technology. *Int. J. Food Sci. Techn.*, **1997,** *32*, 189–201.

[2]   Onsaard, E., Vittayanont, M., Srigam, S., & McClements, D. J. Properties and Stability of Oil-in-Water Emulsions Stabilized by Coconut Skim Milk Proteins. J. Agric. Food Chem. 2005, 53, 5747-5753.

[3]   Tansakul, A., & Chaisawang, P. Thermophysical properties of coconut milk. J. Food Engin., 2006, 73, 276–280.

[4]   le Dean, A., Mariette, F., & Marin, M. 1H Nuclear Magnetic Resonance Relaxometry Study of Water State in Milk Protein Mixtures. J. Agric. Food Chem. 2004, 52, 5449-5455.

[5]   Todt, H., Guthausen, G., Burk, W., Schmalbein, D., & Kamlowski, A. Water/moisture and fat analysis by time-domain NMR. Food Chem. 2006, 96, 436–440.

[6]   Gruwel, M. L. H., Yin, X. S., Edney, M. J., Schroeder, S. W., MacGregor, A. W., & Abrams, S. Barley Viability during Storage: Use of Magnetic Resonance as a Potential Tool To Study Viability Loss. J. Agric. Food Chem. 2002, 50, 667-676.

[7]   Miquel, M. E., & Hall, L. D. Measurement by MRI of storage changes in commercial chocolate confectionery products. Food Res. Int., 2002, 35, 993–998.

[8]   Blümich, B. in NMR Imaging of Materials. (ed. 2). Oxford University Press: Oxford, UK, 2003

[9]   Gibbs,S. J., Haycook, D. E., Frith, W. J., Ablett, S., & Hall, L. D. Strategies for rapid NMR rheometry by magnetic resonance imaging velocimetry. J. Magn. Res. 1997, 125, 43–51.

[10]   Hardy, E. H. in NMR Methods for the Investigation of Structure and Transport. Springer: Berlin, Germany 2011.

[11]   Herold, H., Hardy, E. H., Ranft, M., Wassmer, K.-H., & Nestle, N. Online Rheo-TD NMR for analyzing batch polymerisation processes. Micropo. Mesopor. Mat., 2013, http://dx.doi.org/10.1016/j.micromeso.2013.03.001

[12]   Holz, M., Heil, S. R., & Sacco, A. Temperature-dependent self-diffusion coefficients of water and six selected molecular liquids for calibration in accurate 1H NMR PFG measurements. Phys. Chem. Chem. Phys. 2000, 2, 4740- 4742.

[13]   Adam-Berret, M., Boulard, M., Riaublac, A., & Mariette, F. Evolution of fat crystal network microstructure followed by NMR. J. Agric. Food Chem. 2011, 59, 1767–1773.

[14]   Simuang, J., Chiewchan, N., & Tansakul, A., Effects of fat content and temperature on the apparent viscosity of coconut milk. J. Food Engin. 2004, 64, 193-197.

[15] Peamprasarta, T., & Chiewchan, N. Effect of fat content and preheat treatment on the apparent viscosity of coconut milk after homogenization. J. Food Engin. 2006, 77, 653-658.

[16] Jirapeangtong, K., Siriwatanayothin, S., & Chiewchan, N. Effects of coconut sugar and stabilizing agents on stability and apparent viscosity of high-fat coconut milk. J. Food Engin. 2008, 87, 422-427.

ACKNOWLEDGMENTS